Publicado em: Proceedings do Eurocorr 2004, Nice, France
(14-16 September 2004)

Studies on Sulphuric-Boric Acid Anodising Processes for Aluminium and 2024 Aluminium Alloy

J.C.S. Fernandes[a]*, R. Picciochi[a], M. Da Cunha Belo[a], T. Moura e Silva[b], M.G.S. Ferreira[a,c], I.T.E. Fonseca[d]

[a]*Instituto Superior Técnico, Department of Chemical Engineering, 1049-001 Lisboa, Portugal*
[b]*Instituto Superior de Eng. de Lisboa, Department of Mech. Eng., 1950-062 Lisboa, Portugal*
[c]*University of Aveiro, Dept of Ceramics and Glass Engineering, 3810-193 Aveiro, Portugal*
[d]*CECUL, Faculty of Sciences, University of Lisbon, 1749-016 Lisboa, Portugal*

ABSTRACT

The aim of this work is to show progresses reached with an alternative anodising process for aluminium and aluminium alloys, based in sulphuric/boric baths, under different operating conditions. Traditional processes of chromic acid anodising and sulphuric acid anodising were used as reference.

The corrosion resistance of the anodised materials was determined by electrochemical impedance spectroscopy and outdoor exposure. The present results show that a good protection is achieved with the sulphuric/boric process.

The structure of the oxide films formed on AA2024 with the different anodising processes and its dependence on the anodising and sealing parameters were investigated by scanning electron microscopy and transmission electron microscopy and compared in order to interpret their corrosion performance. The films formed on commercial aluminium using the same anodising conditions were also investigated, as a way for assessing the influence of the alloying elements.

Photoelectrochemical spectroscopy and capacitance measurements were used to assess the electronic properties of anodic oxide films formed by the different processes, in order to obtain information on the electronic structure of these films. The results obtained indicate that the oxide films formed on aluminium show a semiconductive behaviour, with bandgap energies that are identical for the oxides studied, despite their different characteristics. Moreover, from the capacitance measurements performed on commercial aluminium it is possible to ascribe an n-type semiconductive behaviour, in accordance to the literature.

It was found out that capacitance measurements may be used as a valuable technique for the assessment of the quality of anodised layers, allowing the distinction between an efficient and an inefficient sealing. Therefore, they may be used to predict the corrosion resistance of these materials.

Keywords: Aluminium Alloys, Anodising, Capacitance, Photoelectrochemistry

*Corresponding author: Phone: +351 218417964, Fax: +351 218404589, E-mail: joao.salvador@ist.utl.pt

INTRODUCTION

Anodising is a usual process in aeronautical industry for enhancement of anticorrosive properties of aluminium alloys. In the last decade, progress has been made in anodising aluminium using a sulphuric-boric bath as a replacement for the traditional processes of chromic acid anodising (CAA) and sulphuric acid anodising (SAA). Although there is no evidence of a beneficial influence of borate additions in the corrosion resistance of AA 2024-T3 [1], it has been already shown [2,3] that sulphuric-boric anodising (SBA) does not significantly degrade the fatigue properties of the alloy, which is the main drawback of the traditional sulphuric process. Moreover, unlikely the chromic anodising that uses baths containing Cr VI, which are toxic and carcinogenic, the SBA uses an environmentally friendly bath.

In this paper, some results from previous work [4-5] are presented, where the corrosion resistance of the anodised materials was determined by electrochemical impedance spectroscopy and salt spray (CASS) tests, showing that a good protection is achieved with the sulphuric/boric process. The structure of the oxide films formed with the different anodising processes and its dependence on the anodising and sealing parameters have also been investigated by the authors, using scanning electron microscopy and transmission electron microscopy, and compared in order to interpret their corrosion performance.

Following that work, photoelectrochemical spectroscopy and capacitance techniques were used to assess the electronic properties of anodic oxide films formed by the same process, in order to obtain information on the electronic structure of these films that could allow the development of a schematic model for its band structure, which will be published elsewhere. However, during the experimental part of that work it became evident that these techniques may give valuable information on the characteristics of an anodic film, as different patterns are observed for anodised samples prepared under different conditions. Thus, the present paper is mainly intended to show the usefulness of capacitance measurements as a tool for assessing the quality of anodic oxide films.

EXPERIMENTAL

Commercial aluminium (99.0% and 99.5%) and AA 2024-T3 coupons were used. Before being anodised, the specimens were degreased with acetone, followed by etching in 50 $g.l^{-1}$ NaOH solution (2 min, 40°C) and de-smutting in 50% v/v HNO_3 solution (30 sec). The anodising baths were the traditional 15% sulphuric (15% H_2SO_4) and chromic (CrO_3 50 $g.l^{-1}$) baths and a sulphuric-boric bath consisting in a mixture of H_2SO_4 (15%) with a solution containing 0.5M H_3BO_3 and 0.05 M $Na_2B_4O_7.10H_2O$, in the proportion 70/30 (v/v). Sulphuric anodising (SA) was carried out during 30 minutes at 22°C, with a constant current of 1.8 $A.dm^{-2}$. Chromic anodising (CA) was performed at 40°C by sweeping the voltage from 0V to 22 V in the first 5 minutes, followed by 55 minutes at a constant voltage of 22 V. The sulphuric-boric anodising (SBA) process was carried out during 5, 10, 30 or 60 minute at 22°C, with a constant current of 1.5 $A.dm^{-2}$. After anodising, some of the specimens were sealed in boiling reagent grade (Millipore) water for 30 minutes.

Sealed and unsealed specimens were observed on a transmission electron microscope (TEM), in order to assess the different structures of the anodic oxides.

The corrosion behaviour was studied in 3% NaCl solution by electrochemical impedance spectroscopy (EIS), using a Solartron 1250 frequency response analyser and a Solartron 1286 electrochemical interface. Measurements were carried out, at a d.c. potential slightly cathodic

to the corrosion potential (E_{corr} - 20 mV) to avoid deviations in the system linearity [6], by applying to the cell a 10 mV (RMS) sine wave. The frequency range was 50 kHz to 5 mHz.

The performance of the anodised specimens was also evaluated using the copper-accelerated acetic acid salt spray method (CASS test), according to ASTM B 386-97 standard.

Photoelectrochemical measurements were performed, using a 150W xenon lamp, at a fixed potential of 0.75 V (SCE), using a 1200/mm grating monochromator (ORIEL 77200) to sweep the wavelength between 200nm and 700nm. For the measurement of the photocurrent, the beam was chopped at a frequency of 19Hz with a 7505 RI chopper synchronised by an EG&G 5210 lock-in amplifier. Because the flux of photons is wavelength dependent, the photocurrent had to be normalised with respect to the incident flux, which was measured by means of a detector (ORIEL 71832-Si), and a current amplifier (ORIEL 70710). This correction of the measured photocurrent yields the quantum efficiency, η_q, of the photoelectrochemical process.

Capacitance versus potential results were obtained by ac impedance measurements at a fixed frequency of 3160 Hz using a sinusoidal potential wave with an amplitude of 10mV (RMS). Measurements were performed in a potential range of -1.6V to +8V, at intervals of 0.1V, using a 273A EG&G potentiostat and a 5210 EG&G lock-in amplifier.

Both photoelectrochemical and capacitance measurements were performed in 0.5 M Na_2SO_4 solution, where the aluminium / aluminium oxide system is considered to be stable.

RESULTS AND DISCUSSION

a) Anodic Oxide Morphology

A TEM cross-section of an oxide film formed on commercial aluminium in a 15% sulphuric acid bath is shown in Figure 1a. A typical porous structure is observed, where both the barrier layer and the porous layer may be found, as reported by several authors [7-9]. Moreover, the structure of this porous layer is in agreement with the well-established model of cylindrical pores, normal to the metal surface and extending to the outer surface [7-9]. Similar micrographs may be obtained for the oxide film formed on commercial aluminium in the chromic acid bath (Figure 1b), despite the difference in the thickness of the barrier layer and the dimension of the pores, which are higher in this case.

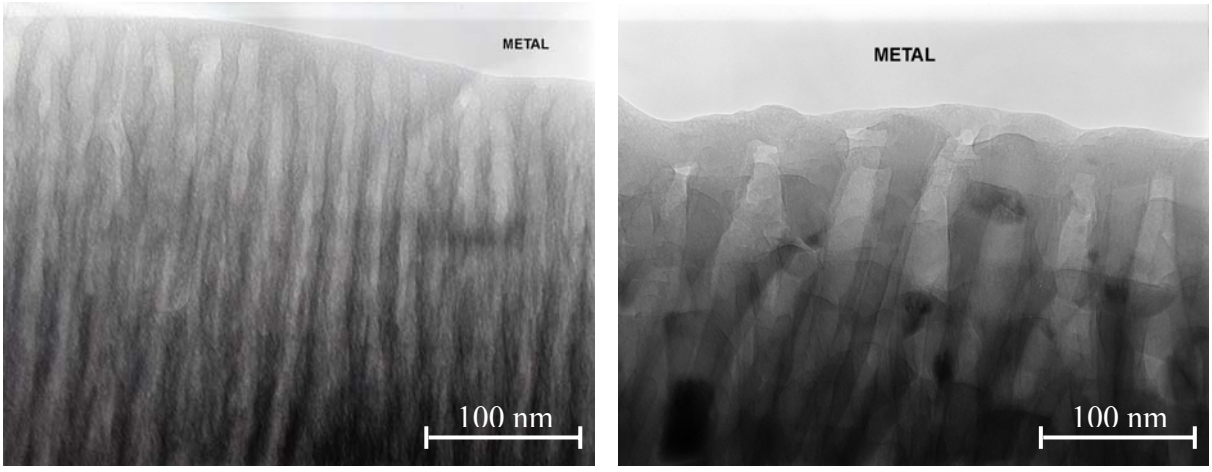

a) b)

Figure 1 – TEM micrographs (200 000 X magnification) of commercial aluminium anodised in: a) sulphuric acid bath:; b) chromic acid bath

However, when the oxide layer is formed on a AA 2024-T3 substrate, its structure changes to a non-oriented grain-like structure were pores perpendicular to the surface can no longer be seen (Figures 2a and 2b), although a barrier layer is still present, being similar to those observed on commercial aluminium (Figure 2b). The reason for the different pore structures may be found on the presence of copper-rich precipitates in alloy, as it is known that they may act as preferential sites for oxygen evolution [10,11]. In fact, a continuous development of oxygen bubbles is always detected during the anodising of the alloy and, although oxygen evolution is a localised process, the mechanical effect of the vertical ascension of the bubbles, parallel to the substrate, may explain the global changes noted on the anodic film.

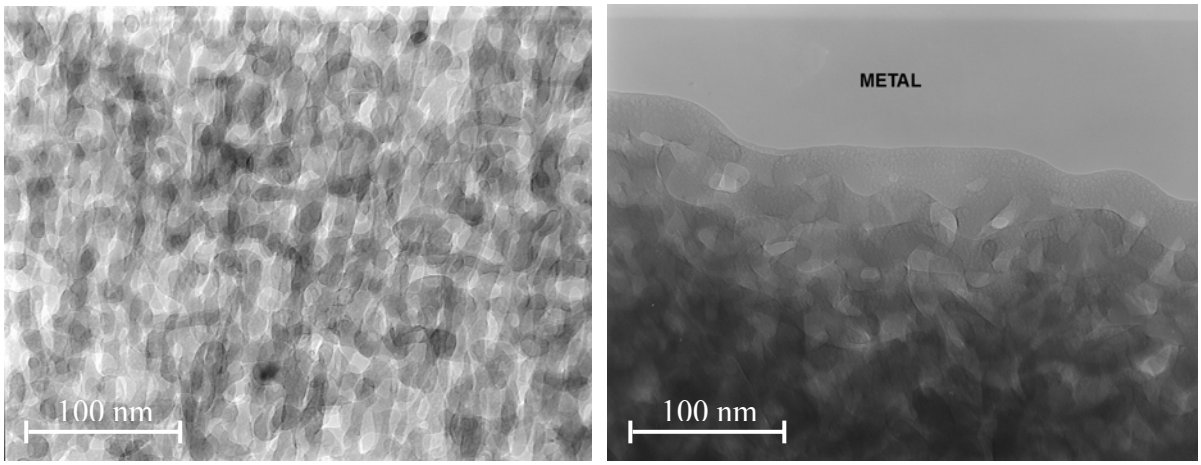

a) b)

Figure 2 – TEM cross-sections (200 000 X) of AA 2024-T3 anodised in:
a) sulphuric acid bath; b) chromic acid bath

The structures obtained for the specimens anodised by the SBA process are quite similar to the ones obtained with the traditional (CA and SA) processes. Different patterns are still observed for commercial aluminium and AA 2024-T3 substrates, as shown in the TEM cross--sections of Figures 3a and 3b.

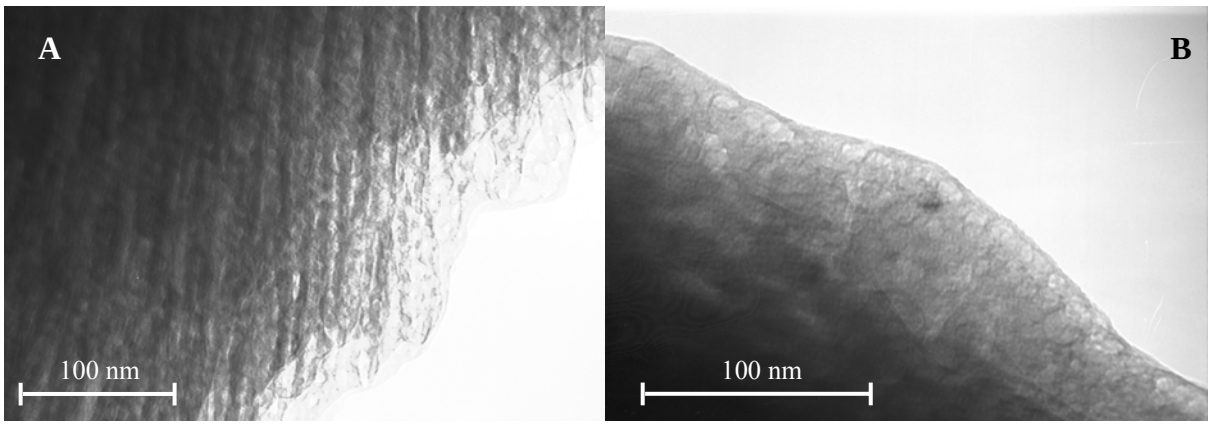

Figure 3 - TEM cross-sections of samples anodised in a sulphuric-boric bath and not sealed:
(A) commercial aluminium - (B) AA 2024-T3

The anticorrosive performance of the different anodising procedures was evaluated by electrochemical impedance measurements in 3% NaCl solution, as described elsewhere [4-5]. For commercial aluminium, the results obtained indicate that no significant differences exist between the three anodising processes, i.e, the impedance values found are similar in all the

cases. The same conclusion was obtained when comparing the results obtained for the AA 2024-T3, meaning that the sulphuric-boric procedure gives an anticorrosive protection which may be considered similar to the one achieved by the classical processes.

However, when comparing the EIS results obtained for sealed samples of the two different materials (commercial aluminium vs. AA 2024-T3), it was found that, regardless the anodising procedure, the effect of sealing is only temporary in the case of the alloy, whereas for commercial aluminium it confers a long time protection. The reason for this difference between the sealing behaviour of AA 2024-T3 and commercial aluminium may be found on the anodic oxide structures observed on the TEM micrographs of the two materials (Figure 3). In fact, the pores formed during anodising of commercial aluminium, which are linear, continuous and perpendicular to the surface, may be easier to seal than the tortuous pores found for the 2024 alloy. In the latter case, the sealing process is less effective and the formation of the hydrated layer is restricted to a superficial zone of the porous oxide, which can be easily penetrated by the solution during exposure to the corrosive environment. Moreover, the different sealing behaviour between commercial aluminium and the 2024 alloy is detected for any of the anodising baths, as the oxide structure is nearly the same for each one of them (Figs. 1-3).

The corrosion performance of unsealed and hot water sealed AA 2024-T3 specimens anodised under the three different procedures was also tested using the copper-accelerated acetic acid salt spray method (CASS test), according to ASTM B 386-97 standard. The sealed samples revealed a higher degree of protection than the unsealed ones, but no significant differences were detected among the CA, SA and SBA processes, indicating that a comparable degree of protection is achieved with the SBA method, relative to the traditional ones.

b) Photoelectrochemical studies

In Figure 1 are presented the results obtained from the photoelectrochemical spectroscopy measurements performed on commercial aluminium, as-received and after 60 minutes SBA anodising, unsealed and hot water sealed.

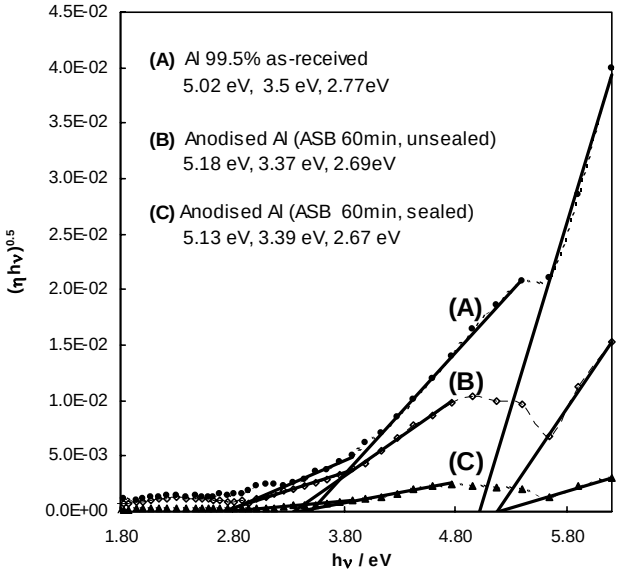

Figure 4 – $(\eta h\nu)^{0.5}$ vs incident light energy plots, obtained in 0.5 M Na_2SO_4 , for commercial aluminium: (A) as-received; (B) after 60 min SBA, unsealed ; (C) after 60 min SBA, hot water sealed.

Apparently, a semiconductive behaviour of the oxide films obtained in all the three conditions is found, since a photocurrent was measured which at this applied potential is anodic [12].

The photoelectrochemical response of a semiconductor is dependent on its electronic structure. Taking into account the Gärtner model [13] and introducing some simplifications [14], the quantum efficiency η_q for semiconducting electrodes, defined as the ratio between the photocurrent I_{ph} and the incident photon flux ϕ_o, is given by the following relationship:

$$\eta_q = \frac{I_{ph}}{\Phi_o} = eAw\frac{\left(h\nu - \mathcal{E}_g\right)^n}{h\nu}$$

where A is a constant, e the elementary charge, w the space charge layer thickness, $\mathcal{E}_g$ the bandgap energy and hν the photon energy. The value of n depends on the type of transition between the valence and conduction band and in this work it was assumed n = 2, corresponding to indirect optical transitions. However, other kind of transitions is not ruled out and is being considered for future work.

In each one of the spectra of Figure 4 three different regions may be defined where a linear relationship between $(h\nu\eta_q)^{0.5}$ and hν is observed. From the fitting of these regions it is possible, according to the above equation, to determine values of transition energies, which are identical for the three oxides, despite their different characteristics. In fact, the untreated aluminium of Figure 1A is only covered by a thin natural oxide film, with a maximum thickness of about 15 nm [15,16], whereas in the two other cases thick oxide films of a few microns were produced during the anodising process. Moreover it is interesting to note that the photocurrent spectra obtained for the anodised aluminium is practically independent of the sealing, being the major difference related with the quantum efficiency values. The lower value obtained for the sealed material can be ascribed to a higher recombination rate of the hole-electron pairs created by the incident photons, as hole transport through a thicker layer is more difficult [12].

The interpretation of the photocurrent spectra, namely the presence of three distinct extrapolation energies, is very complicated, as transitions from bandgap states (electron traps) into the conduction band, transitions from the valence band to bandgap states (hole traps), transitions from the valence band to the conduction band and transitions from surface states to the conduction band have to be considered. Furthermore, there is an important controversy concerning the interface where photoeffects are controlled [17]: the metal/oxide interface, by means of photoinjection processes (i.e., transitions from the Fermi level of the metal to the conduction band in the oxide film), or the space charge region of the oxide/electrolyte interface, by the creation of hole-electron pairs. In the present work, photoinjection must be ruled out, since it would result in cathodic photocurrents, whereas the values obtained are anodic.

Concerning the two lower values of energy levels determined for the different samples, they are very similar to those found in the literature [17-19], with a slight shift towards lower energies that could be related to different surface preparation [18]. Di Quarto et al [19] also obtained two low energy transitions in the photocurrent spectra, at ca 3 eV and 3.5 to 3.7 eV. According to these authors, the two values can be originated by the presence, in the outer part of the internal oxide film, of two hydrated layers with different hydration contents. On the other hand, the higher transition found at ca 5.15 eV is in the energy range of the various values reported in the literature for the bandgap of anhydrous Al_2O_3 (5.1 to 8.7 eV, increasing with the cristallinity degree [17,20]). Thus, the photoelectrochemical response of the passive film under irradiation would arise from the contributions coming from three different phases

with hydration contents increasing from the inner to the outer layer and, therefore, presenting different optical gaps and photocarriers transport properties.

In order to clarify the above points-of-view and to obtain information on the electronic structure of these anodic oxide films that could allow the development of a schematic model for its band structure, a more fundamental approach is still being followed, which will be published elsewhere.

b) Capacitance measurements (Mott-Schottky approach)

It is well established that the capacitance behaviour of a semiconductor-electrolyte interface is similar to that of a semiconductor-metal Schottky junction [21]. Thus, the effect of the applied potential E on capacitance values is described by the Mott-Schottky equation:

$$\frac{1}{C^2} = \frac{2}{\varepsilon\varepsilon_0 q N_d}\left(-E + E_{fb} + \frac{kT}{q}\right)$$

where N_d is the carrier concentration (donor or acceptor), ε the dielectric constant of the semiconductor, ε_0 the vacuum permittivity, q the elementary charge (-e for electrons and +e for holes), k the Boltzmann constant, T the temperature and E_{fb} the flatband potential. This equation predicts a linear C^{-2} vs E plot where the point of intersection with the E-axis gives the flatband potential.

In Figure 5a it is presented a C^{-2} vs E plot obtained for commercial aluminium, as-received, in 0.5 M Na_2SO_4 solution. As it can be seen, the capacitance values decrease with the applied potential, leading to the development of a straight line with positive slope in the C^{-2} vs E plot. This fact indicates an n-type semiconducting behaviour for the natural Al oxide, in agreement with the literature [22,23] and with the photoelectrochemical results presented above.

The influence of film growth during the potential sweep used for the capacitance measurement must not be ignored, as it could account for a decrease in the capacitance values. However, the present results depict a linear relationship between C^{-2} and E, which is typical of a semiconductor, whereas pure film growth would lead to a linear plot of 1/C vs. E

For commercial aluminium samples anodised by the SBA process and hot water sealed (Figure 5b), the C^{-2} vs. E plot presents a quite different shape, as C^{-2} is constant in the entire potential range, indicating a dielectric behaviour of the oxide film. This different behaviour, when compared with the natural aluminium oxide, may be due to the increased thickness of anodic oxide and to its duplex structure. Considering that the capacitance measured in this case is the result of a series arrangement of two capacitances associated with each one of the oxide layers and that the porous layer shows a lower capacitance [5,7,24], the Mott-Schottky plot will only reflect the contribution from this layer. Thus, even if the inner layer presents a semiconductive behaviour, generating a photocurrent, its response in the Mott-Schottky measurements may not be detectable.

Moreover, constant capacitance values obtained in this case are characteristic of the anodic oxide film produced and show a strong dependence on the anodising time. In fact, assuming that the insulating film behaves as a parallel plate capacitor, its capacitance C will depend on the thickness d, in the form $C = \varepsilon\varepsilon_o/d$. As the anodising procedure results in the formation of a duplex anodic film, whose porous layer thickness is proportional to the anodising time, and the subsequent sealing closes efficiently the pores, longer anodising times will then produce a thicker dielectric with lower capacitances and, though, higher values of C^{-2}.

For commercial aluminium samples anodised by the same SBA process but unsealed, the C^{-2} vs E plot (Figure 5c) reveals a similar dielectric behaviour, but in this case the constant capacitance values obtained are almost identical, independent of the anodising time and much higher than the ones obtained for sealed anodic oxides. The reason for this behaviour may be found on the duplex structure of the anodic film, which in this case was not sealed. As the presence of pores leads to a short-circuiting of the response of the porous oxide, the capacitance measured is only related to the barrier layer. On the other hand, the maximum thickness of the barrier oxide is reached during the first few seconds of anodising [12], meaning that it have been obtained for all these samples, regardless the anodising time. Thus, the associated capacitance is expected to be the same, as observed.

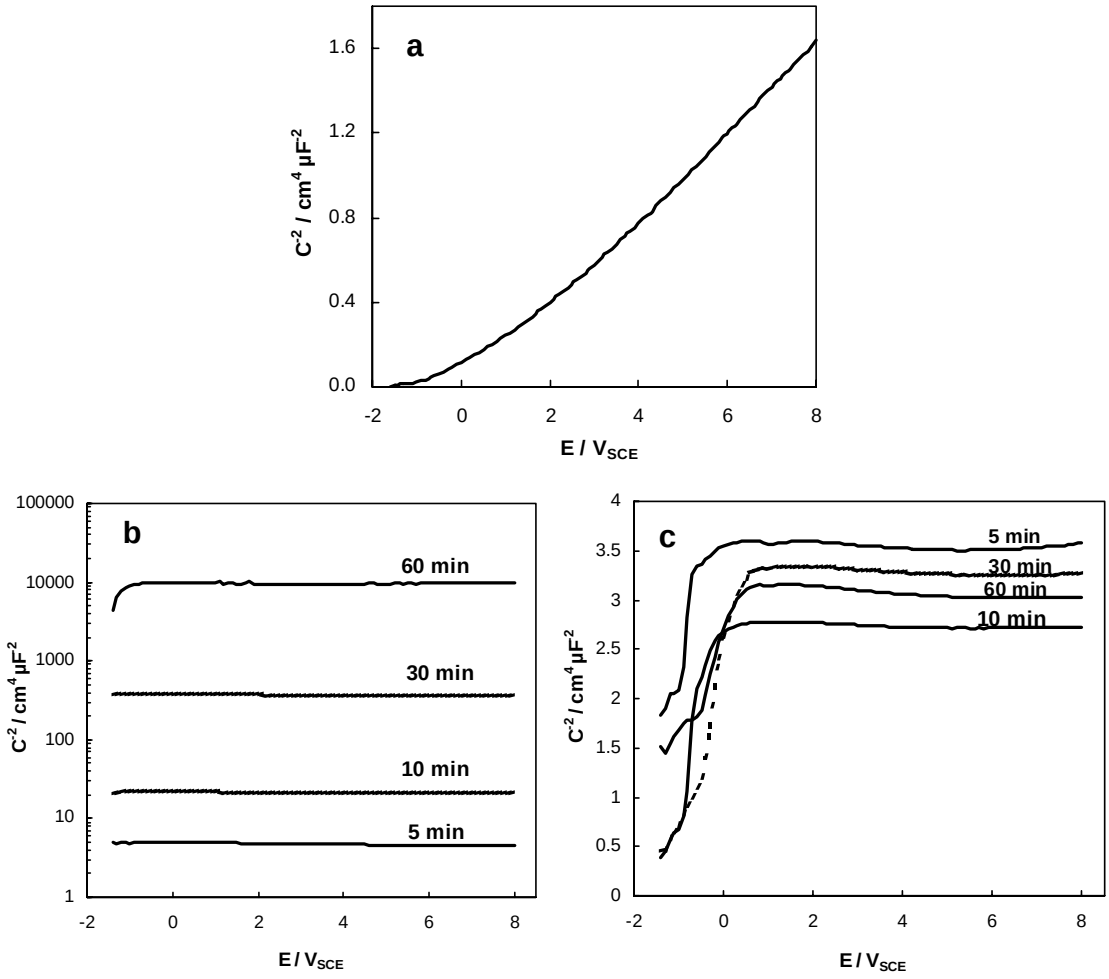

Figure 5 – C^{-2} vs E plots, obtained in 0.5 M Na_2SO_4 solution, on commercial aluminium: (a) as-received; (b) after SBA (5 min, 10 min, 30 min and 60 min anodising) and hot water sealing; (c) after SBA (5 min, 10 min, 30 min and 60 min anodising), unsealed.

The capacitance results obtained in the same solution for the aluminium alloy 2024-T3 anodised by the SBA process with different anodising times and unsealed are presented in Figure 6a. With the exception of an initial step, up to approximately –200 mV (vs SCE), which could be attributed to the presence of active copper-rich precipitates that become oxidized for higher potentials, the oxide behaves as an insulator, showing horizontal C^{-2} vs E lines. Similarly to commercial aluminium, no influence of the anodising time is detected, which may be explained by the same arguments, i.e., for a unsealed duplex anodic oxide the capacitance response measured is due to the barrier layer, whose thickness is independent of the anodising time.

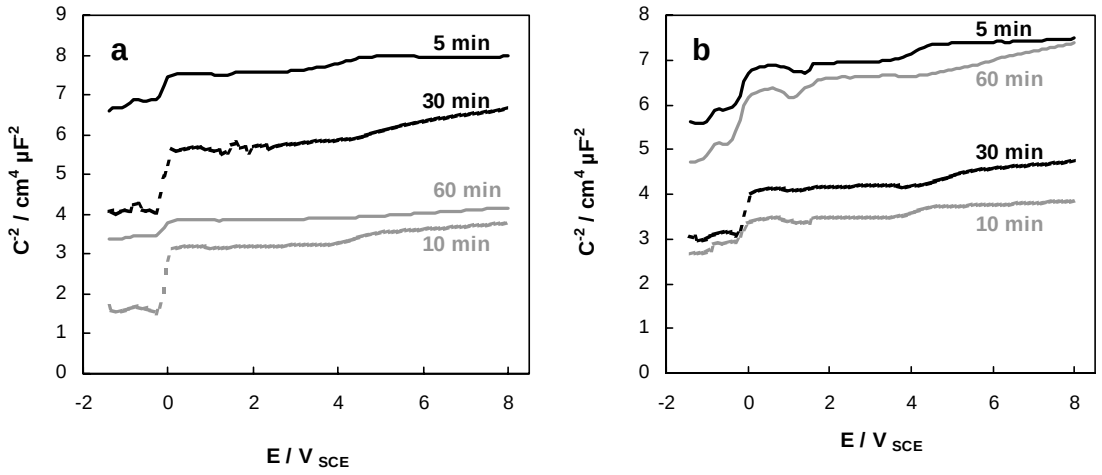

Figure 6 – C^{-2} vs E plots, obtained in 0.5 M Na_2SO_4 solution, for aluminium alloy 2024-T3 after SBA (5 min, 10 min, 30 min and 60 min anodising): (a) unsealed; (b) hot water sealed.

For the Al 2024-T3 samples anodised by the SBA process and hot water sealed, the C^{-2} vs E plots (Figure 6b) are quite similar to those obtained for the unsealed material and, in particular, no dependence on the anodising time is observed. The reason for this different behaviour of the 2024-T3, compared with the commercial aluminium, is again related with the anodic oxide structures of the two materials and its impact on the sealing process, as mentioned above. On the alloy the sealing process is not efficient and the sealed specimens tend to behave similarly to the unsealed ones.

In this perspective, capacitance measurements may be regarded as a useful technique for the assessment of the quality of anodised layers. As shown above, this method allows the distinction between an efficient and an inefficient sealing and therefore it may be used to predict the corrosion resistance of these materials.

CONCLUSIONS

The anodic films formed on AA 2024-T3 by chromic acid, sulphuric acid and sulphuric-boric acid anodising exhibit a non-oriented grain like structure, with tortuous pores that are not perpendicular to the surface. On the contrary, for commercial aluminium, the same procedures lead to oxide structures in agreement with the well-established model of cylindrical pores, normal to the metal surface and extending to the outer surface. The different structure observed for the AA 2024-T3 may be explained as the effect of oxygen evolution occurring preferentially on the copper-rich precipitates that are present in this alloy. This non-oriented pore structure is responsible for the hindering of the sealing process on the alloy, which is not extended to the whole thickness of the porous layer. Thus, only a thin superficial hydrated layer is formed, which is easily destroyed when in contact with an aggressive solution.

From the EIS and CASS tests results, no significant differences were found in the corrosion performance obtained by the three anodising methods in each material, i.e., the BSA anodised specimens show protective properties that can be considered similar to the ones obtained with chromic acid anodising or sulphuric acid anodising.

It was also concluded that capacitance measurements may be a valuable technique for the assessment of the quality of anodised layers. For non-anodised aluminium the semiconductive behaviour of its natural oxide was clearly revealed, whereas the anodised materials have shown a dielectric response in the C^{-2} vs E plots. Moreover, this response is very sensitive to

the changes of the oxide film occurred during the sealing procedure, revealing that this process is ineffective in the case of the 2024-T3 alloy. Thus, it may be concluded that capacitance measurements allow the distinction between an efficient and an inefficient sealing and, therefore, may be used to predict the corrosion resistance of these materials.

REFERENCES

1. G.E. Thompson, L. Zhang, C.J.E. Smith and P. Skeldon, *Corrosion*, **55**, 1052 (1999)
2. L. Domingues, J.C.S. Fernandes, M.G.S. Ferreira, T. David, L. Guerra-Rosa, I.T.E. Fonseca, Proc. 14th International Corrosion Congress, Cape Town, (1999), 237,1
3. L. Domingues , J.C.S. Fernandes, M.G.S. Ferreira, I.T.E. Fonseca, *Cor. Prot. Mat.*, **18**, 13 (1999)
4. L. Domingues, J.C.S. Fernandes and M.G.S. Ferreira, Proc. 15th ICC, Granada, Spain (2002), Paper 444
5. L. Domingues, J.C.S. Fernandes, M. Da Cunha Belo, M.G.S. Ferreira, L. Guerra-Rosa, *Corros. Sci*., **45** (2003) 149
6. F. Mansfeld, J.C.S. Fernandes, *Corros. Sci*., **34**, 2105 (1993).
7. T.P. Hoar, G.C. Wood, *Electrochim. Acta*, **7**, 333 (1962)
8. S. Tajima, in "*Advances in Corrosion Science and Technology*", Vol. 1, Chap.4, M.G. Fontana and R.W. Staehle Eds., Plenum Press, New York (1970)
9. G.E: Thompson, H. Habazaki, K. Shimizu, M. Sakairi, P. Skeldon, X. Zhou and G.C. Wood, *Aircraft Eng. and Aerospace Tech.*, **71**, 228 (1999)
10. J.R. Galvele and S.M. De Micheli, *Corros. Sci.*, **10**, 795 (1970)
11. T. Dimogerontakis, L. Kompotiatis and I. Kaplanoglou, *Corros. Sci.*, **40**, 1939 (1998)
12. J.C.S. Fernandes, R. Picciochi, M. Da Cunha Belo, T. Moura e Silva, M.G.S. Ferreira, I.T.E. Fonseca, submited to *Electrochim. Acta*
13. W.W. Gärtner, *Phys. Rev.*, **116** (1959) 84
14. Y. Pleskov, Y. Gurevich, in "Modern Aspects of Electrochemistry", B.E. Conway, C.R. White and J.O'M. Bockris Eds., Vol. 16, Plenum Press, New York (1985)
15. J.E. Graedel, *J. Electrochem. Soc.*, **136** (1989) 204C
16. R.S: Alwitt, *J. Electrochem. Soc.*, **121** (1974) 1322
17. F. Di Quarto, C. Gentile, S. Piazza, C. Sunseri, *J. Electrochem. Soc*., **138** (1991) 1856
18. G. Tuccio, S. Piazza, C. Sunseri, F. Di Quarto, *J. Electrochem. Soc*., **146** (1999) 493
19. S. Piazza, C. Sunseri, F. Di Quarto, *Corrosion*, **58** (2002) 436
20. J.P. Sukamto, C.S. McMillan, W. Smyrl, *Electrochem. Acta*, **39** (1993) 15
21. Y. Pleskov, Y. Gurevich, in "Semiconductor Photoelectrochemistry", P.N. Bartlett Ed., Consultants Bureau, New York (1986)
22. E. Mc Cafferty, *Corros. Sci.*, **54** (2003) 301
23. J.O'M. Bockris, Y. Kang, *J. Solid State Electrochem.*, **1** (1997) 17
24. F. Mansfeld and M.W. Kendig, *J. Electrochem. Soc.*, **135**, 828 (1988)

Acknowledgements – The authors acknowledge the Portuguese Science and Technology Foundation (FCT) for the financial support under the Operational Programme of Science, Technology and Innovation (POCTI). The financial support of this work through contract nº PRAXIS/3/3.1/CTAE/1919/95 is also greatly acknowledged